

Interferometry of Actuated Microcantilevers to Determine Material Properties and Test Structure Nonidealities in MEMS

Brian D. Jensen, Maarten P. de Boer, Nathan D. Masters, Fernando Bitsie, and David A. LaVan

Abstract—By integrating interferometric deflection data from electrostatically actuated microcantilevers with a numerical finite difference model, we have developed a step-by-step procedure to determine values of Young's modulus while simultaneously quantifying nonidealities. The central concept in the methodology is that nonidealities affect the long-range deflections of the beams, which can be determined to near nanometer accuracy. Beam take-off angle, curvature and support post compliance are systematically determined. Young's modulus is then the only unknown parameter, and is directly found. We find an average value of Young's modulus for polycrystalline silicon of 164.3 GPa and a standard deviation of 3.2 GPa ($\pm 2\%$), reflecting data from three different support post designs. Systematic errors were assessed and may alter the average value by $\pm 5\%$. An independent estimate from grain orientation measurements yielded 163.4–164.4 GPa (the Voigt and Reuss bounds), in agreement with the step-by-step procedure. Other features of the test procedure include that it is rapid, nondestructive, verifiable and requires only a small area on the test chip. [619]

Index Terms—Free-standing thin films, *in situ* characterization, mechanical properties, statistical accuracy assessments.

I. INTRODUCTION

KNOWLEDGE of mechanical properties is critical to the design of MEMS. Nanoindentation [1] is commonly used to determine properties of thin films attached to a substrate, but substrate compliance and tip shape effects introduce considerable complexity into analysis methods (see, for example, [2] and references, therein). Free standing thin-film structures are

Manuscript received September 5, 2000. This work was supported by the United States Department of Energy under Contract DE-AC04-94AL85000, where Sandia National Laboratories is a multiprogram laboratory operated by Sandia Corporation, a Lockheed Martin Company. Subject Editor W. N. Sharpe, Jr.

B. D. Jensen was with the MEMS and Novel Silicon Science & Technology Department, Sandia National Laboratories, Albuquerque, NM 87185 USA. He is now with the Department of Mechanical Engineering, University of Michigan, Ann Arbor, MI 48109 USA.

M. P. de Boer is with the MEMS and Novel Silicon Science & Technology Department, Sandia National Laboratories, Albuquerque, NM 87185 USA (e-mail: mpdebo@sandia.gov).

N. D. Masters was with the MEMS and Novel Silicon Science & Technology Department, Sandia National Laboratories, Albuquerque, NM 87185 USA. He is now with the Department of Mechanical Engineering, Brigham Young University, Provo, UT 84602 USA.

F. Bitsie is with the Electromechanical Engineering Department, Sandia National Laboratories, Albuquerque, NM 87185 USA.

D. A. LaVan was with the Mechanical Reliability and Melting Department, Sandia National Laboratories, Albuquerque, NM 87185 USA. He is now with the Massachusetts Institute of Technology (MIT), Cambridge, MA 02139 USA.

Publisher Item Identifier S 1057-7157(01)05033-8.

routinely fabricated as part of a MEMS process flow. Load is applied to test such structures by mechanical [3]–[6], dynamic [7], [8] and electrostatic methods [9]–[11]. However, although the film is directly interrogated, it has proven difficult to obtain consistent values for such basic quantities as Young's Modulus, E . Early reported values of E varied from 90 to 190 GPa [12] for polycrystalline silicon (polysilicon), which is the most common structural material used in MEMS. A recent round-robin study in four laboratories [13] showed variation in measured values of E from 132 to 174 GPa for different measurement techniques applied to structures fabricated side-by-side on the same chip.

There are several sources for these large discrepancies. First, there may be some material differences in polysilicon from one fabrication facility to another. A difference in crystalline orientation from [1 0 0] to [1 1 1] can account for a change of 130 to 188 GPa in the expected value of E , as calculated from the bulk elastic stiffness constants [14]. The film density and average orientation are affected by film deposition and annealing parameters, changing E by up to 10% [15]. However, literature reports [5], [16] and results of this investigation indicate that annealed polysilicon texture is nearly isotropic, and hence that $E \sim 163$ GPa is expected. Therefore, second and more importantly, uncertainties and nonidealities at the microscale also affect the measurements of free standing structures. For example, tensile testing is sensitive to misalignment of the loading apparatus which can be a source of systematic error [17]. Damping introduces uncertainty into dynamic methods unless the measurements are carried out in a vacuum. Dynamic methods must also separate out effects of boundary compliance, similar to the beam bending approaches discussed next.

Static approaches involving cantilever bending have been investigated by mechanical [6] and electrostatic loading methods [9]–[11]. A difficulty in the mechanical bending test is that a tip must be aligned to and sense a compliant cantilever. Only short stiff cantilevers can be sensed, and support post compliance can be responsible for a large fraction of the deflections [6]. Scanning load-control techniques can overcome this limitation, but require knowledge of the unloaded beam deflection [18]. The electrostatic loading method has the advantage that well calibrated low voltages generate small forces (nano- to micronewtons) that can be accurately calculated provided that the deflections are well known. Typically, highly compliant beams are used and the "pull-in voltage," reflecting an electromechanical instability, is used to infer basic properties such as Young's Modulus. Electrostatics is the usual means to actuate MEMS devices and alignment of electrical probes to nearby pads is

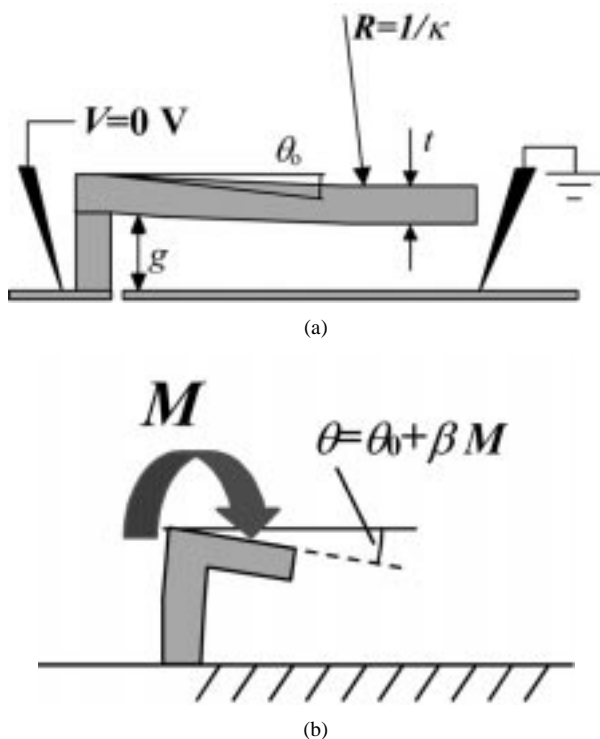


Fig. 1. (a) Thickness t , gap g and nonidealities θ_0 (unloaded beam end angle) and κ (curvature due to intrinsic stress gradient, R is the radius of curvature) in the unloaded cantilever beam. (b) Nonideality β (torsional compliance) in the loaded beam. θ is the loaded beam angle the applied moment is M (for $V > 0$ V).

routine. Therefore, this method has both theoretical and practical advantages. Nonetheless, the method still has drawbacks when it comes to assessing the impact of nonidealities on the measured property value. In “M-Test” pull-in experiments [10], the stress gradient nonideality was circumvented by fabricating structures that did not exhibit film curvature κ [see Fig. 1(a)], and single crystal films with well-known modulus values were used. In most micromachined cantilevers, the Young’s modulus is not known *a priori*. Nonidealities such as nonzero κ , nonzero takeoff angle θ_0 [19]–[23] [Fig. 1(a)] and nonzero support post torsional compliance β [Fig. 1(b)] are always present. Expanding on [10], Gupta [16] has calculated the effect of nonidealities such as κ and β on pull-in voltage. Calculated values of such nonidealities are directly inserted, or are found by determining a best fit to pull-in voltage data for a series of test structures, usually ten in number. Fundamental parameters such as E are then determined. However, if the values of the nonidealities are not the same as those calculated, or if different nonidealities exist from those assumed, the results will be systematically skewed. An important example is that of nonzero θ_0 .

In this paper, we introduce a step-by-step procedure to measure and validate properties of microcantilever beams by integrating deflection data of unloaded and loaded beams with test structure models. The key to the method is that deflections are measured to the nanometer scale while actuating the structures. Electrostatic force calculations, which depend on knowing the gap spacing, are then accurate. Furthermore, because κ , θ_0 and β affect global deflections of the cantilever, they can be systematically quantified and then inserted into the model. Vali-

ation is achieved by demonstrating repeatable values of E at various applied voltages and beam lengths. Another advantage of this test methodology is that it is nondestructive, useful in assessing the effect of subsequent process steps such as packaging on stress (the pull-in test often results in adhesion of the device, and therefore the test cannot be repeated). Also, only one cantilever is necessary to obtain all of these values (although use of three cantilevers improves accuracy). This is important because more area on the wafer can then be dedicated to MEMS applications.

We present an overview of the step-by-step procedure to measure nonidealities and determine Young’s modulus in Fig. 2. The gap g and thickness t of the cantilever are measured in Step 1. In Step 2, the deflection curve of the unloaded beam is measured by interferometry. In Step 3, the unloaded beam angle θ_0 and curvature κ are deduced by finding the most probable values of (θ_0, κ) that fit the measured deflection curve. In Step 4, deflections of actuated beams are measured by interferometry. In Step 5, with the previously measured values of g , t , θ_0 and κ inputs to the model, a value for loaded beam takeoff angle θ is determined at each voltage loading by finding the most probable values of (θ, E) that fit the actuated beam deflection curve. Initial values of E result. In Step 6, a value of the moment M at each voltage loading is calculated. Plotting θ versus M , a regression fit is made to determine β according to the equation shown in Fig. 1(b). Improved values for E are then determined. In the following sections, we present experimental procedures, the modeling approach, results and a discussion of systematic errors.

II. EXPERIMENTAL

A. Test Structure Design and Processing

Test structures were designed and fabricated using Sandia National Laboratories’ multilevel surface micromachining technology (SUMMiT) [24]. Polysilicon, which makes up both the beams and the ground plane, is deposited amorphously by low pressure chemical vapor deposition at 580 °C with *in situ* phosphorous doping. A high temperature anneal before polysilicon etching recrystallized and reduced stress, so that microstructure is constant across the width of the cantilevers. The beams and the ground plane are electrically isolated from the silicon substrate and each other by a 0.6- μm layer of thermal oxide under a 0.8- μm layer of low-stress nitride. The test structure array consisted of nine cantilever beams of 700, 500, and 300 μm , with three different support post designs. One cantilever of each length was fabricated with each support post design. The width of each beam is 20 μm . The cantilevers were fabricated in the Poly 3 level, with nominal thickness and gap of 2.25 and 6.5 μm , respectively. After processing, the structures were released in HF acid and rendered freestanding by supercritical drying.

SEM images of the three support posts and schematics of their cross sections are shown in Fig. 3(a)–(c). The cross sections are shown perpendicular to the beam’s length. The support posts consist of two layers of polysilicon (Poly 2 and Poly 3) and two layers of sacrificial oxide (Sacox 1 and Sacox 3). These deposited oxide layers are thermally densified before subsequent polysilicon depositions, and develop a compressive stress sim-

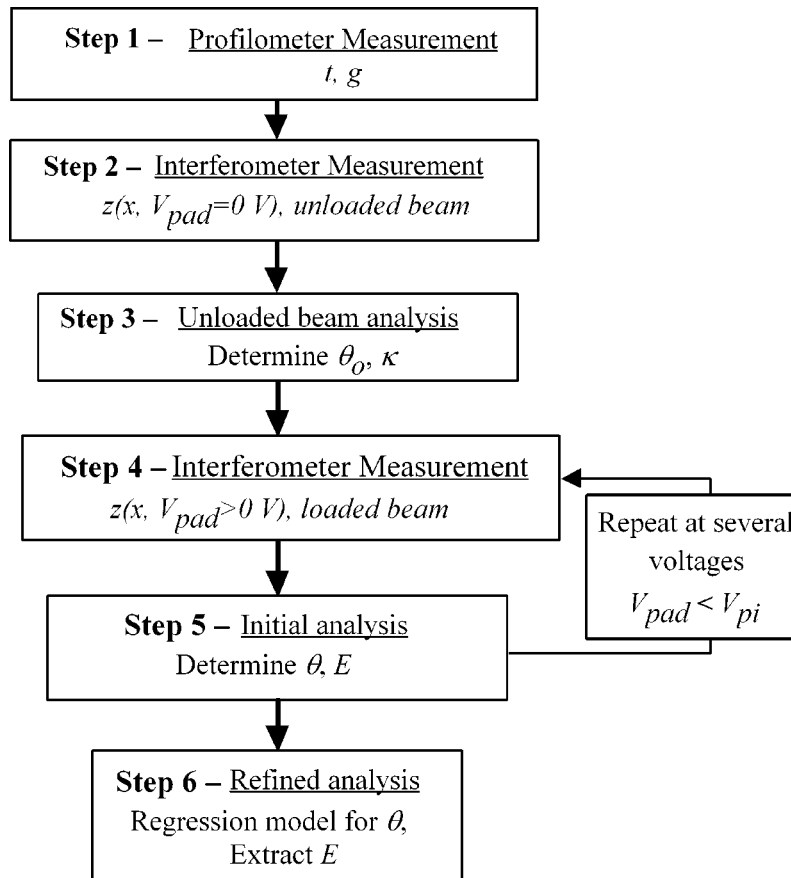


Fig. 2. Step-by-step procedure to quantify mechanical properties and nonidealities of thin-film cantilever beams.

ilar to thermally grown oxide (~ 300 MPa). Chemical mechanical polishing (CMP) planarizes the Sacox 3 layer to a thickness of approximately $2 \mu\text{m}$ above the top of Poly 2. Thus, Pad 1 as shown in Fig. 3(a) is formed as follows. First, a large square cut is made in Sacox 1, and Poly 2 is deposited over it. Because of the CMP process, Sacox 3 is thick over the recessed Poly 2 area. Sacox 3 is also defined by a large square cut, but the oxide not fully etched away during the Sacox 3 dry etch. The result is a step up support post encompassing a $\sim 2\text{-}\mu\text{m}$ -thick oxide. Pad 2, shown in Fig. 3(b), includes long, narrow cuts in the Sacox 1 layer. These cuts are parallel to the direction of the beam. When Poly 2 is deposited over these narrow cuts, it fills conformally, leaving ripple-like topography on the top surface of Poly 2. Then, a large, square cut is made in planarized Sacox 3, and Poly 3 is deposited. The result is a pad with a step-up post that is not as tall as that in Pad 1, and incorporates oxide only under Poly 2. Pad 3 has long, narrow cuts in Sacox 1 similar to Pad 2. It also has long, narrow cuts in Sacox 3 that are staggered over those in Sacox 1. The step-up geometry is further reduced for this post. It has an oxide volume approximately the same as Pad 1, but the oxide material is highly constrained by the Poly 2 and Poly 3.

B. Interferometry

Deflections of the microcantilever beams are measured using a Michelson interferometer with an incoherent tungsten halogen light source filtered by a 547-nm green light interference filter.

Green light is only weakly transmitted through silicon, eliminating problems with secondary fringes caused by transmitted light reflecting from the substrate. Error caused by reference surface misalignment is minimized by adjusting its tilt until substrate fringes are parallel to the beam's length. Movement of fringes is a sensitive measure of when the probe contacts the surface. After detection of contact, no further pressure was applied by the probe tips so that substrate or pad deformation would not induce deflections in the cantilevers. Deflections of unloaded cantilevers measured before and after probe contact are indistinguishable. A Keithley 487 picoammeter/voltage source was used to apply voltages. Currents were below the 1 pA level.

Interferograms are recorded on an eight bit gray scale CCD camera (640×480 pixels). A computer program was developed to convert the linescan intensity data along a beam's length into out-of-plane deflection versus position data. The program finds local minima and maxima in the linescan, which establish deflection differences of $\lambda/4 \approx 137$ nm. Relative deflections at each pixel between these loci are interpolated using an arc-cosine function [25], yielding near nanometer scale data. The program requires beam direction (up or down) and inflection point information to be input by the user. This is inferred by focusing up and down (or by shifting the reference surface position), and noting the direction of fringe movement. The result is a pixel-by-pixel deflection curve along the beam's length ($\sim 2.6 \mu\text{m}$ per pixel when a $5\times$ objective is used). Occasionally, parts of the linescans may have noise due to particles on the beams or rapid changes in topography if the beam passes over a

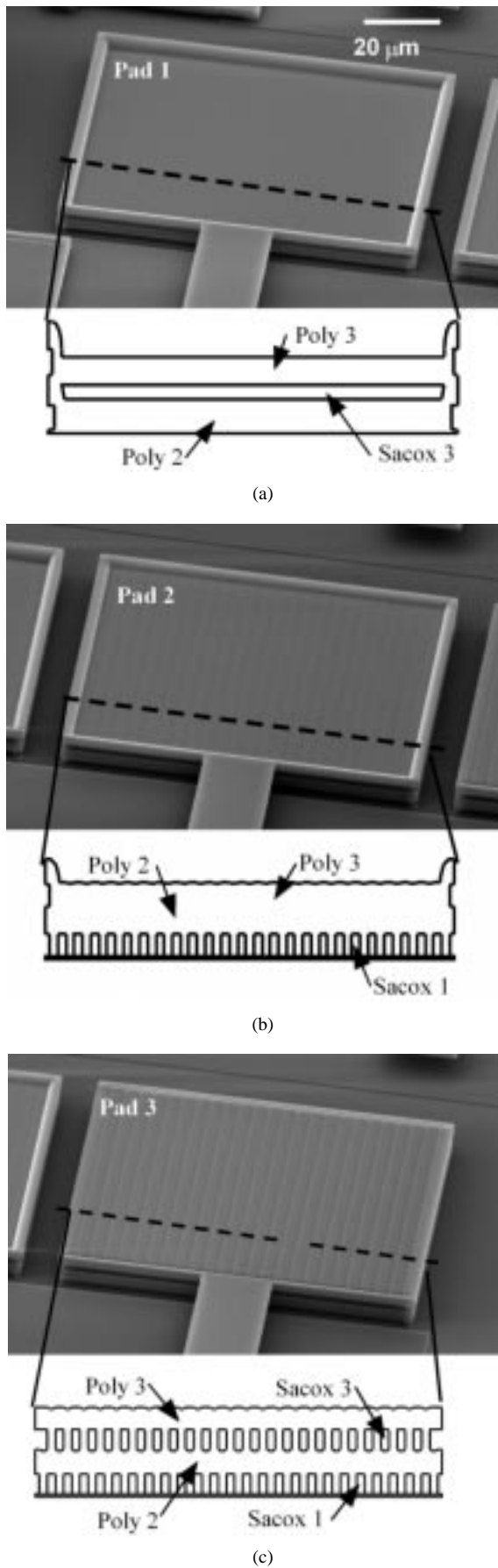


Fig. 3. SEM and schematic cross-section views of (a) Pad 1, (b) Pad 2, and (c) Pad 3.

short gap in the underlying polysilicon. This noisy data usually accounts for only a small percentage of the total beam deflection curve; therefore it may be dropped from the data provided that the relative pixel count is properly maintained.

III. MODELING

A. Cantilevers

A cantilever beam model was implemented using the finite difference method (FDM). The model is based on the Bernoulli-Euler equation,

$$\frac{\partial^2 z}{\partial x^2} = \frac{M}{EI} + \kappa \quad (1)$$

where

- M internal moment in the beam;
- I area moment of inertia of the beam cross section;
- z out-of-plane deflection (away from the substrate is taken to be positive);
- x ; distance from the support post along the cantilever length.

The internal moment M is found by dividing the beam into a number of small elements along its length. The electrostatic force acting on each beam element is then computed as a function of deflection, allowing calculation of the internal moment at each node using equilibrium equations.

The electrostatic force acting on each element is a function of the deflection of that element. Similarly, the deflection of each element is a function of the electrostatic forces acting on the beam. Therefore, the beam deflection model iterates on the deflection solution until a specified level of convergence is reached. The electrostatic force must also be corrected to include the effects of fringing fields acting on the sides of the beam. We use the correction from [10], given as

$$F_e(x) = \frac{\epsilon_o}{2} \left(\frac{V}{g+z(x)} \right)^2 \left[1 + 0.65 \left(\frac{g+z(x)}{w} \right) \right] \quad (2)$$

where

- $F_e(x)$ electrostatic force at x ;
- ϵ_o dielectric constant of air;
- w beam width;
- V applied voltage.

For cantilever beams, the effective modulus \tilde{E} rather than Young's modulus E is measured. According to finite element modeling [16], \tilde{E} for the case of uniform pressure loading in cantilevers is

$$\frac{1}{\tilde{E}} = \frac{1}{E} - \frac{\nu^2}{E} \left[\frac{(\frac{w}{L})^{1.37}}{0.5 + (\frac{w}{L})^{1.37}} \right]^{0.98(L/t)^{-0.056}} \quad (3)$$

where ν is Poisson's ratio, which is assumed to be 0.23 for polysilicon. For typical beam geometries in this work, $E \sim 0.996\tilde{E}$. Note that this correction is significantly smaller than $E \sim (1 - \nu^2)\tilde{E} = 0.947\tilde{E}$ for wide beams representative of plane strain conditions, indicating that the sensitivity to the value of ν assumed is weak.

Many investigations [19]–[23] have demonstrated that the unloaded beam takeoff angle, θ_0 , can be different from zero due to

stress relaxation at the support post. The deflection curve of an unloaded beam is approximated by

$$z(x) \approx \theta_0 x + \kappa \frac{x^2}{2}. \quad (4)$$

Equation (2) neglects gravity, which plays a small role with $\rho_{\text{Si}} = 2.3 \text{ kg/m}^3$, but gravity is included in the finite difference code.

Besides θ_0 and κ , torsional support post compliance β [Fig. 1(b)] affects global deflections. With $\theta_0 \neq 0$, a linear equation for the beam end angle is assumed with

$$\theta = \theta_0 + \beta M \quad (5)$$

where M is the moment at the support post.

For an unloaded (loaded) beam, most probable values of θ_0 and κ and (θ and E) are determined by a quasi-Newton search algorithm nested within the finite difference code. The algorithm minimizes the deflection difference in the rms error per pixel between the measured and modeled deflections. While the interferometry gives extremely good relative deflection data, three physically based corrections must be made to compare the model and measured deflections. First, the deflection curve from interferometry gives values of deflection relative to the first x -pixel. Topography near the support post beam transition area prevents interferometry data from being gathered at the very beginning of the beam. Instead, the measured deflection curve is usually extracted beginning about five pixels from the beam's true beginning. A measured x -offset is applied to the measured deflection data so that the data reflects the actual position from the beam's beginning. Also, the beam deflection at this first measured pixel cannot be $z = 0$ for beams with known nonzero deflections. We have applied a z -offset such that the first measured point lies on the modeled curve. Second, a calibration factor for the length per pixel must be determined. Because magnification is sensitive to focus, but depth of field is large for the low numerical aperture objective used here, the x -calibration factor must be determined each time beams are brought into focus. The calibration was done on the longest beam length of $700 \mu\text{m}$. With negligible linewidth loss of $\sim 0.1 \mu\text{m}/\text{edge}$ after processing, a typical calibration is $2.62 \mu\text{m}$ per pixel for the $5\times$ ($NA = 0.09$) objective used. Third, if the substrate fringes are not parallel to the beam length, a linear correction that is calculated from the relative rotation can be applied. In these experiments, this correction was insignificant and therefore not applied.

B. Finite Element Modeling of Supports

To gain further insight into the pad stiffnesses, each support pad design was modeled using three-dimensional (3-D) finite element method (FEM) analysis to calculate β . The measured thickness and gap were used in the FEM analysis. A deformed mesh for Pad 1 is shown in modeled Fig. 4. The modeled β values of 1.37 , 1.24 , and $1.30 \mu\text{rad}/(\mu\text{N}\bullet\mu\text{m})$ for Pads 1, 2, and 3, respectively, indicate an expected compliance for comparison with measured values. Although the three pads react very differently to axial loads (modeled axial compliances varied by a factor of three [23]), their angular deflections in response to a

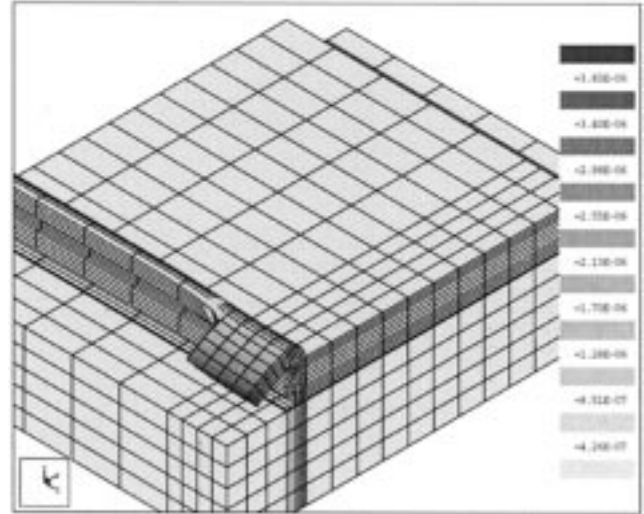


Fig. 4. Finite element predictions of pad deflection for Pad 1 under an applied moment. The deflection is magnified for clarity.

moment load are almost identical. The small effect is because all three pads have an identical $1 \mu\text{m}$ overhang due to the design rules, which require a minimum overlap of polysilicon over an oxide cut. However, as we shall see, the three pads have significantly different θ_0 values.

IV. RESULTS

A. Step-by-Step Procedure

We now proceed through the step-by-step analysis outlined in Fig. 2. Carrying out Step 1, calibrated contact profilometry measurements indicated a film thickness of $2.28 \mu\text{m}$, with a gap of $6.62 \mu\text{m}$ between the beams and the underlying electrodes. For this step, the stylus of the profilometer was swept over a raised polysilicon pad to find the combined thickness of the gap and polysilicon layer. The end of the beam that was pushed down to the ground plane was then measured to find the thickness of the polysilicon beams. Subtraction provided the gap height. (Step 1 was actually carried out after Step 4) to avoid damage to the test structures. However, with noncontacting optical profilometry, it is possible to perform this step first).

Using interferometric deflection measurements of unloaded beams from Step 2, the beam end angle θ_0 and film curvature κ were found according to Step 3. An example is given in Fig. 5. The interferometry technique relies on having at least one half fringe available, so that a maximum and minimum intensity in the linescan are well known. Because the cantilevers are quite flat, only the $700\text{-}\mu\text{m}$ beams exhibited sufficient deflection for measurement of intrinsic curvature. It should be noted in Fig. 5(b) that the deflection data begins only at $x = 260 \mu\text{m}$. The reason the data begins here rather than near $x = 0$ is that the minimum in the linescan at $x = 260 \mu\text{m}$ is indicative of a change in the deflection slope from negative to positive, as can be determined by the splitting of fringes at this point focus is changed. The first maximum in the linescan is larger than the next one, making it cumbersome to extract the deflections correctly before this point (this can be caused by a small illumination nonuniformity or finite illumination coherence length). As

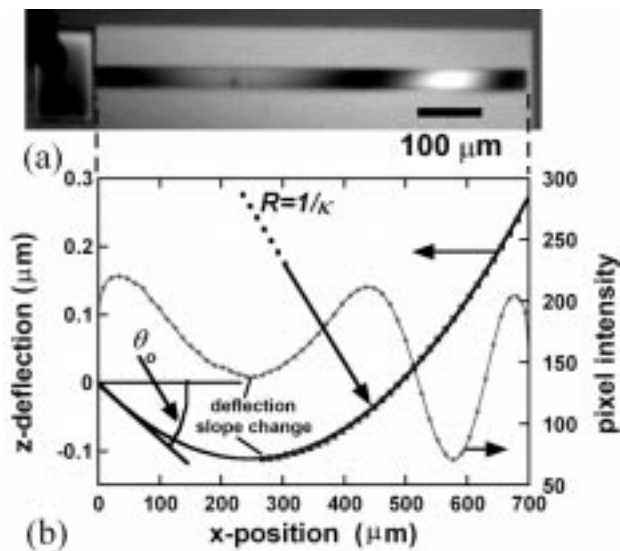


Fig. 5. (a) Interferogram of an unloaded cantilever beam. (b) Corresponding gray-scale pixel intensity linescan, measured and best-fit modeled deflection curve (Pad 1, $L = 700 \mu\text{m}$).

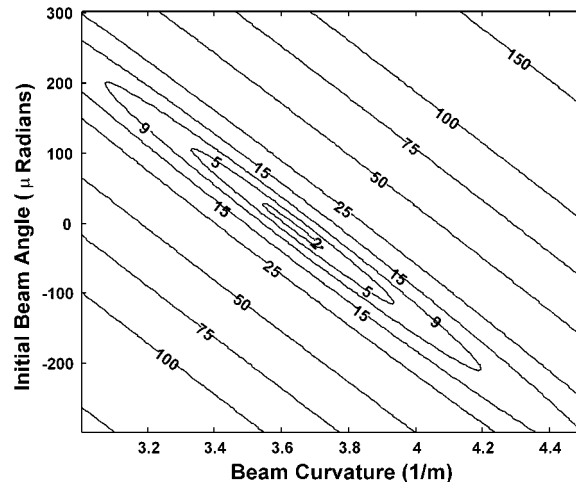


Fig. 7. The most probable values of θ_0 and κ lie at the minimum in this contour plot of the error (nm/pixel) between model and measurement of an unloaded beam. (Pad 2, $L = 700 \mu\text{m}$).

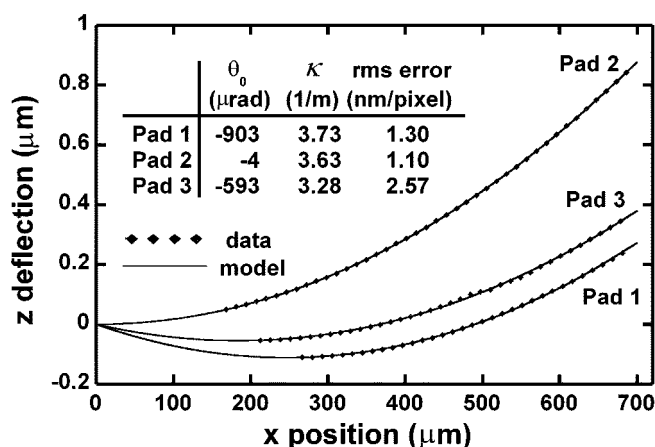


Fig. 6. Measured and modeled deflection curves of unloaded beams for each pad design. (Every fifth measured data point is shown).

θ_0 and κ both affect the global deflection curve, the modeling can be carried out because the data is still taken from a significant fraction of the beam.

Fig. 6 shows the measured and modeled deflection curves for each pad. The pad designs produce different unloaded beam end angle θ_0 (negative θ_0 represents rotation toward the substrate). Fig. 7 is a contour map of the rms per pixel difference between the model and measured data where model κ and θ_0 values are varied. The most probable value is at the minimum in this plot.

Deflections of actuated beams were next measured, according to Step 4. For this step, deflection measurements were made for each undamaged beam (the $300 \mu\text{m}$ beam attached to Pad 2 became stuck to the ground plane during the release and drying procedure, and the $700\text{-}\mu\text{m}$ beam attached to Pad 3 was damaged during deflection measurements). Deflection data from each of the remaining seven beams was gathered in this step, using three or four voltage levels per beam. According to Step 5, takeoff angle θ and initial E values were determined. The polysilicon etch profile in the SUMMiT process gives an

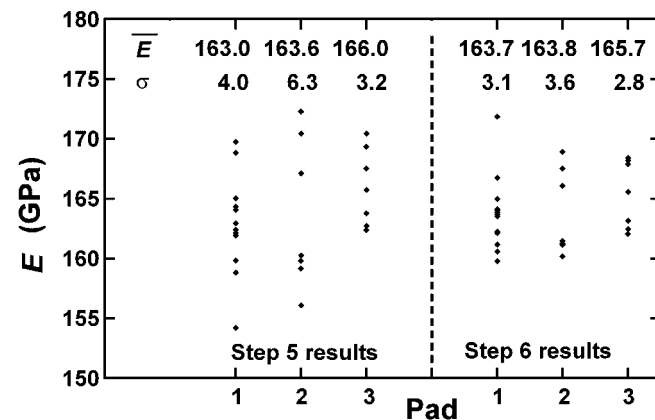


Fig. 8. Young's modulus results for Step 5 (left) and Step 6 (right) analyses. The average and standard deviations are 163.9 ± 4.5 and 164.3 ± 3.2 GPa for Steps 5 and 6, respectively.

$89\text{--}89.5^\circ$ sidewall, and therefore no geometrical correction is necessary to I . Surface roughness as measured by atomic force microscopy is $2\text{--}5$ nm rms for the upper and lower electrodes, and is insignificant in the force calculations considering the $4\text{--}6 \mu\text{m}$ gap. Each pair of (θ, E) values at a given voltage is taken from the most probable value in a contour plot, with g , t , and κ determined previously. Young's Modulus results are shown on the left-hand side of Fig. 8. Average values of E agree for the three pad types. Grouping the populations together, the overall average and standard deviation for the 27 data points on the left hand side of Fig. 8 are 163.9 ± 4.5 GPa after the Step 5 analysis.

A typical contour plot showing the rms error per pixel between the model and the data for one particular voltage loading is shown in Fig. 9. Because many data points are taken to determine the deflection curve, the contours can be associated with confidence levels. Using the F -distribution function [26], the 95% confidence contour within which the values of θ and E lie is also shown in Fig. 9, indicating that the θ value is $935 \pm 50 \mu\text{rad}$ and that the E value is 164 ± 4 GPa. The 95% interval reflects the confidence based only on the deflection data,

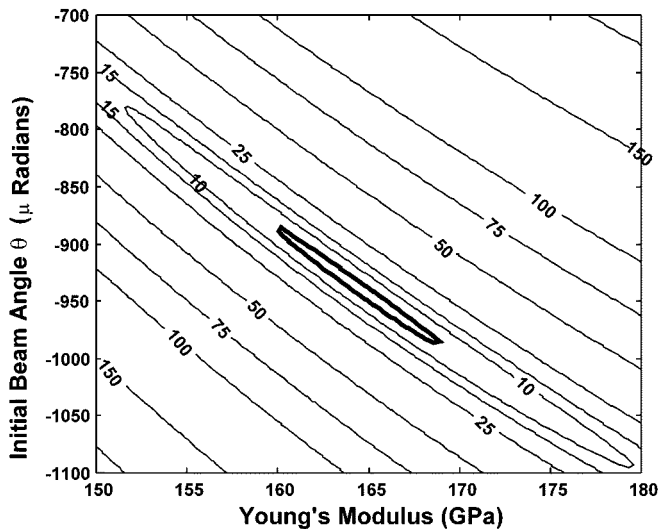


Fig. 9. The most probable values for θ and E lie at the minimum in this contour plot of the error (nm/pixel) between model and measurement of the loaded beam. The minimum error is 2.76 nm/pixel and the 95% confidence contour (thick line) is at 4.45 nm/pixel. (Pad 1, 700- μm beam, 6.96 V applied).

and not uncertainty from other sources. The f -value is determined from the ratio $(\sigma_{\text{rms}}/\sigma_{\text{min}})^2$, where σ_{rms} is the error per pixel between the model and the measured value, and σ_{min} is the minimum or best fit error. If each of the measured deflection data points were independent, there would be $(N - 1)$ degrees of freedom dof , where N is the number of pixels in the linescan across the length of the beam. Larger dof reduces the area of the 95% contour. We have used $dof = 0.05N$ (rather than $N - 1$) to determine the critical f -value for the 95% confidence contour because a power spectrum analysis indicates there is some correlation in the deflection data and that $0.05N$ better represents dof . One reason for dof not approaching N is thermal noise in the pixel intensity measurements. Nonsystematic errors in the location and value of linescan extremes (where the intensity is slowly varying) may be introduced, affecting the deflection curve extraction.

Although a reasonable value of E has been determined after Step 5, the standard deviation can be reduced by a further consideration. That is, the values of θ determined in Step 5 likely lie within the 95% confidence intervals but are subject to nonsystematic error. However, they must be related by the linear nature of the support post according to (5). At each voltage loading, the value of M can be calculated from the deflection curve. Plotting the values of θ versus M as in Fig. 10, a least-squares linear regression fit yields a weighted value of θ_0 (the y -intercept) and a value for β (the slope). The solid lines in Fig. 10 show the regression fit to the data for each pad design. The dotted lines show the slope predicted by the finite element modeling (offset so that the slopes can be compared). The regression equations in the form of (5) and their correlation coefficients r^2 are

Pad	Least squares fit	r^2 value	
1	$\theta = -829 + 1.90M$	0.89	(6a)
2	$\theta = 31 + 1.33M$	0.47	(6b)
3	$\theta = -281 + 2.09M$	0.91.	(6c)

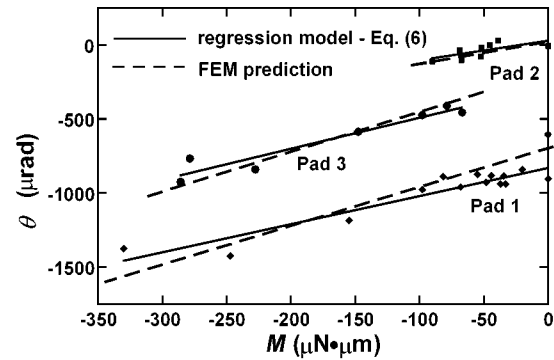


Fig. 10. Loaded beam end angle θ versus end moment M for each pad. Dashed line fit from FEM is offset to allow comparison of slopes (β) to regression model.

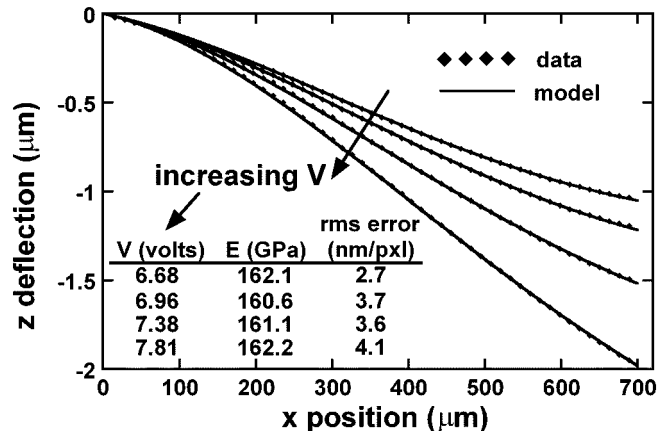


Fig. 11. Modeled and measured deflections at several voltages. The only free parameter in the model fit is E (Pad 1, $L = 700\text{-}\mu\text{m}$ beam, every fifth data point is plotted).

In (6) the units for θ are μrad and for M are $\mu\text{N} \cdot \mu\text{m}$. Note in Fig. 10 that the range of data for Pad 2 is smaller than the others because the 300 μm beam attached to this pad type was damaged. As this is the stiffest beam, larger moments can be applied to it before pull-in. Because data from this beam was not obtainable, the Pad 2 data is more concentrated, and the associated r^2 value is smaller. For Pad 3, the value for θ_0 is not used in the regression, because it is an outlier. Hence, the weighted data yields an improved value of θ_0 .

With β modeled according to (6), E is found in a single-parameter fit using the same deflection data as in Step 5. The result, summarized on the right hand side of Fig. 8, shows that the scatter in E is decreased. Again, average values of E agree well for the three pad types. Grouping the values together, the overall average and standard deviation for the 27 data points on the right hand side of Fig. 8 are 164.3 ± 3.2 GPa. Based on the Step 6 model values, we show in Fig. 11 modeled versus measured deflection curves of a 700- μm cantilever beam at different actuation voltages. This beam is attached to Pad 1. Typical errors are 3–4 nm/pixel, and are slightly greater than in Step 5 (1–3 nm/pixel), because θ is no longer a free parameter.

B. Grain Orientation Measurements

Young's modulus was also estimated using the Electron Backscatter Kikuchi Pattern (EBKP) technique [27]. This

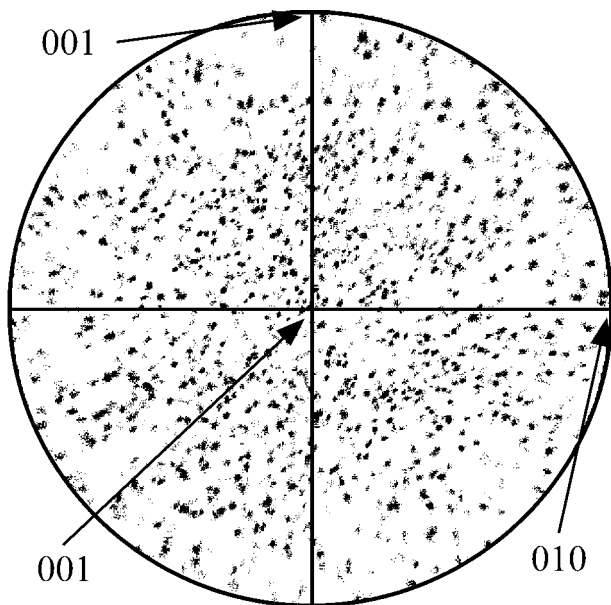


Fig. 12. Pole figure indicating random grain orientation of the polysilicon. data obtained from electron backscatter Kikuchi Pattern (EKBP) grain orientation method.

measurement was performed on polysilicon produced in the same facility using the same process as that used for the earlier measurements, and could resolve orientations on grains as small as $0.1 \mu\text{m}$. Although the grain structure was columnar, a nearly isotropic distribution of grain orientations was found as seen in Fig. 12 based on a sample size of 67 identified grains of $\sim 0.1\text{--}2 \mu\text{m}$ size. Using the equation indicated in [28], an expected value for the in-plane value of Young's modulus, appropriate for the applied experimental strain, between 163.4 and 164.4 GPa (Voigt and Reuss bounds) was found using the elastic constants for single crystal silicon.

V. DISCUSSION

Although the support post compliance β did not vary greatly between pads designs as determined by FEM and corroborated by the experiments, the takeoff angle θ_0 depends on the pad design. By examining Fig. 3, it is seen that θ_0 as reported in (6) correlates with the amount of incorporated sacrificial oxide near the top of the pad. This suggests that nonzero θ_0 is induced by relaxation of the compressive oxide incorporated in the pad during the HF release step for these support pads. In principle, it is possible to calculate values of θ_0 in the FEM model by analyzing the stress that develops in the deposited oxide layers as a function of the anneal cycles. Such work has been carried out for simpler pad geometries [21]. For the more complicated geometries here, this calculation is beyond the scope of the present work. In any case, θ_0 is well measured by the procedure.

Because each beam is fabricated in the same polysilicon layer and near the other beams (within $800 \mu\text{m}$), each beam should have the same value for Young's Modulus in spite of the different θ_0 values. An important result of the above analysis is that the Young's modulus is the same for the three support post designs. The fdm code allows us to calculate the effect of θ_0

on pull-in voltage V_{pi} . For a $500\text{-}\mu\text{m}$ -long beam, the V_{pi} will be 15.89 V for $\theta_0 = 0$ and 14.54 V for $\theta_0 = -1000 \mu\text{rad}$ (assuming otherwise the same other values as in Table I). Because Young's Modulus is assumed to be proportional to V_{pi}^2 for pull-in testing [10], an error of 19% in E can result. Those errors would be reduced by modeling and measuring pull-in voltages over a large number of test structures as done in [10], [16], but by directly measuring deflections, improved validation is achieved.

The mechanics of electrostatically actuated beams are highly nonlinear, and therefore obtaining accurate property values depends strongly on obtaining accurate values for g , t , θ_0 , κ and the applied electrostatic force. Values for g and t can be obtained to $\sim \pm 0.02 \mu\text{m}$ accuracy from a calibrated profilometer or an optical interferometer. Reasonable values for θ_0 and κ were demonstrated here, but required some adjustment. Namely, the values of θ_0 in (6) were weighted by obtaining data at multiple loading conditions. Also, κ was averaged from the data of Pads 1 and 2 only before proceeding to Step 5. This was justified by the observation that the Pad 3 unloaded θ_0 data is incorrect, and that its κ data does not closely agree with Pads 1 and 2. Further, it should be noted that the fdm algorithm adjusts the z -offset at the first point in the data to be equal to the model value, and then finds the best model fit to the data. This causes an ambiguity in the absolute z -deflection values. For loaded beams, there was no inflection point and the data was taken beginning 5 pixels from the support post (see, for example, Fig. 11). This tends to minimize the z -offset ambiguity compared to the unloaded beam data. Although small, reducing z -offset ambiguity error through improved measurement procedures is clearly desirable. We are now investigating support post designs that have no topography, which allows measurement of the full deflection curve.

Systematic error can be introduced from three other sources described at the end of Section III-A-i) the position of the initial pixel in the data may be incorrectly offset by 1 or 2 pixels relative to the true position, ii) the pixel calibration (x -length/pixel) may be incorrect by 1 or 2 pixels in 267 (the number of pixels in the $700\text{-}\mu\text{m}$ long beam at the magnification used), and iii) small rotation of the substrate fringes relative to the beam direction will result in a θ_0 error (we estimate a 5° maximum rotation error of substrate fringes relative to the beam direction).

For uniform loading, $E \propto qL^4/(t^3 \bullet z(L))$, implying systematic errors of $1 - (q'/q)(L'/L)^4(t/t')^3[z(L)/z(L')]$ in the accuracy of E , where the primed variable results from the experimental evaluation, and the unprimed variable is the true value. For example, if the first pixel is incorrectly offset by two, then $L' = 500 + 2 \bullet (700/267) \mu\text{m} = 505.2 \mu\text{m}$, giving an error of 4.2% in E . Likewise, a rotation error of the substrate fringes of less than 5° relative to the beam length is difficult to detect. This can result in a $\Delta\theta_0$ error of $50 \mu\text{rad}$ (assuming the substrate fringes are separated by $\sim 200 \mu\text{m}$). For $z(L) \approx g/3 = 2 \mu\text{m}$, $z(L') = 2.025 \mu\text{m}$ using (4), and an error of 1.3% in E results. We estimate a curvature resolution of $\sim \pm 0.1 \text{m}^{-1}$ from the interferometry. The same error of 1.3% in E occurs if κ is incorrect by 0.15m^{-1} . Because the deflection measurements reflect bending stiffness = $Et^3/12$, a $\pm 0.02 \mu\text{m}$ error in thickness measurements affects E by $\pm 2.5\%$. The accuracy of the force, (2), depends on the accuracy of $(g + z(L))$ to approximately the

TABLE I
EFFECT OF SYSTEMATIC ERRORS ON ACCURACY¹

Type of error	Estimated Max Error	ΔE	$\Delta\beta$
Incorrect x -offset	± 2 pixels	$\mp 3.5\%$	$\mp 97.1\%$
Incorrect calibration	± 2 parts in 267	$\pm 0.7\%$	$\pm 8.0\%$
Rotation of substrate fringes	$\pm \Delta\theta_0 = 50 \mu\text{rad}$	$\mp 0.7\%$	$\mp 0.3\%$
Curvature κ	$\pm \Delta\kappa = 0.15 \text{ m}^{-1}$	$\mp 3.1\%$	$\pm 1.0\%$
Thickness t	$\pm \Delta t = 0.02 \mu\text{m}$	$\mp 2.5\%$	$\mp 0.0\%$
Gap g	$\pm \Delta g = 0.02 \mu\text{m}$	$\mp 0.7\%$	$\pm 0.5\%$
Voltage V	$\pm (0.1\% + 4 \text{ mV})$	$\pm 0.3\%$	$\pm 0.5\%$
All of the above	(rms estimate)	$\mp 5.4\%$	$\mp 97.4\%$

¹ Table calculations for model beam data assume $\kappa = 3.5 \text{ m}^{-1}$, $\theta_0 = -500 \cdot \text{rad}$, $t = 2.25 \mu\text{m}$, $g = 6.50 \mu\text{m}$, $L = 500 \cdot \text{m}$, $\beta = 2 \mu\text{rad}/(\mu\text{N} \cdot \mu\text{m})$, $E = 164 \text{ GPa}$ and that the model data begins at $x = 10 \mu\text{m}$. The pull-in voltage for this case is $V_{pi} = 15.27 \text{ V}$. Percent changes after shifting data were calculated from E or β averaged over $V = 8, 12,$ and 15 V after the Step 6 analysis.

third power. Near the pull-in voltage, the deflection accuracy is $(2/3) \bullet 6.62 \pm 0.02 \mu\text{m}$, yielding a $\pm 1.4\%$ change in E from force errors. The accuracy of the Keithley 487 voltage source is specified to be $\pm(0.1\% + 4 \text{ mV})$. For $V_{pi} = 15.27 \text{ V}$, an error in E of 0.3% results assuming $E \propto V_{pi}^2$.

The errors are better calculated by providing model data to the finite difference code, and shifting it according to these estimated systematic errors to determine how much E is changed. Errors in β can then also be assessed. The results of such calculations are shown in Table I. The largest errors of $\pm 3.5\%$ and $\pm 3.1\%$ are associated with incorrect x -offset and κ respectively. Because these errors are independent, a root mean square calculation as in the bottom row of Table I applies, and a systematic error in E of $\pm 5.4\%$ results. It should be noted that if lower voltages are used, errors in E increase significantly because of a strong sensitivity to an incorrect evaluation of κ , especially for long beams. Therefore, E is best evaluated closer to the pull-in voltage. For the calculations in Table I, the same voltages as those used experimentally were assumed.

Of interest in the top row of Table I is the $\pm 97\%$ change in β due to a two pixel x -offset error. This can be understood in a sense as a book-keeping issue in that the support post/beam boundary is being repositioned, which obviously changes the effective compliance. More precisely, the model is attempting to fit to a noticeable change in θ , implying that the extracted values for β depend strongly on the choice of x -offset from the interferogram. Even if the best pixel is chosen, sub-pixel errors will affect the accuracy of β . Because the percentage error of β is linear with small errors in x -offset, the agreement of $\sim 50\%$ between the measured and FEM calculated values of β is reasonable and implies that the x -offset used was ~ 1 pixel from the true x -offset. Comparison of the measured β value to the FEM value is a good criterion for establishing if the best value of x -offset was used. Furthermore, imprecision in the measured value of β does not strongly affect the value of Young's Modulus, and therefore FEM analysis of support post compliance is not required if only a good evaluation of Young's Modulus is desired.

In terms of small standard deviation, low systematic error and close agreement with the grain texture assessment, [5] is among

the best reported in the literature by the tensile testing technique ($11.5 \mu\text{m}$ thick films). Our results for E of $164.3 \pm 3.2 \text{ GPa}$ (one standard deviation) from 27 measurements in Step 6, systematic errors of $\pm 5.4\%$ and an expected $E = 163.4$ – 164.4 GPa from grain texture measurements are comparable to [5] for tensile testing. There, $E = 164.5 \pm 4.9 \text{ GPa}$ was determined from 32 measurements, systematic errors at $\pm 5\%$ were assessed, and a value of $E = 162.7 \text{ GPa}$ from grain texture was inferred. Our results compare favorably with the best pull-in testing results on polycrystalline silicon currently in the literature [16], where $E = 155 \pm 10 \text{ GPa}$ was found for a single run, while grain texture measurements yielded an expected value of $E = 163 \text{ GPa}$.

VI. CONCLUDING REMARKS

We have demonstrated a procedure that integrates modeling techniques with nanometer scale measurement to determine mechanical properties and nonidealities of actuated microcantilevers. The technique lends itself to various statistical analyzes of accuracy. The 95% confidence area in the contour plot for θ and E , which gives the measurement uncertainty based on the deflection data, allows us to evaluate which system enhancements will be most effective in further improving measurement resolution. Two other assessments (Steps 5–6 and the systematic considerations) show that the accuracy of the technique is currently 5.4% or better for E . The value of $164.3 \pm 3.2 \text{ GPa}$ (one standard deviation) from Step 6 is in good agreement with the expected value from 163.4 to 164.4 GPa from grain texture measurements. Best results for E are obtained by accurately determining curvature κ and making measurements at voltages near the pull-in voltage. Equation (5) for β is best evaluated over a large range of M , which can be obtained from beams of several different lengths. The value of β is sensitive to small errors in x -offset, but this does not strongly affect the value of E . Therefore, finite element simulations of support post compliances are not needed to insure that E is accurately evaluated by this method.

We have recently demonstrated an integrated platform to determine mechanical properties by this method at the wafer

scale [29]. Along a wafer column, we found little variation in E (~ 161 GPa), but significant changes in κ and residual stress. Presently, we can measure and analyze the properties discussed here in approximately two working days along a wafer column (eight locations). Further improvements in measurement speed and accuracy are expected. An important feature of the integrated platform is that many properties critical to MEMS can be measured on the same test instrument. Namely, interferometry in concert with properly designed and analyzed test structures is also useful in accurately assessing residual stress [22], [23], adhesion (i.e., stiction) [30], [31], adhesion hysteresis (of silane coatings in dry and wet environments) [32], friction [33], [34] and fracture strength [35].

ACKNOWLEDGMENT

The authors would like to acknowledge the staff of the Microelectronics Development Laboratory at Sandia National Laboratories for their fabrication work. They also thank E. V. Thomas for discussions on aspects of the statistics and M. S. Baker for help in carrying out some of the measurement and error analysis.

REFERENCES

- [1] W. C. Oliver and G. M. Pharr, "An improved technique for determining hardness and elastic-modulus using load and displacement sensing indentation experiments," *J. Mater. Res.*, vol. 7, no. 6, p. 1564, 1992.
- [2] J. A. Knapp, D. M. Follstaedt, S. M. Myers, J. C. Barbour, and T. A. Friedmann, "Finite element modeling of nanoindentation," *J. Appl. Phys.*, vol. 85, no. 3, p. 1460, 1999.
- [3] W. N. Sharpe, B. Yuan, and R. L. Edwards, "A new technique for measuring the mechanical properties of thin-films," *J. Microelectromech. Syst.*, vol. 6, p. 193, Sept. 1997.
- [4] T. Tsuchiya, O. Tabata, J. Sakata, and Y. Taga, "Specimen size effect of tensile strength of surface-micromachined polycrystalline silicon thin films," *J. Micromech. Microeng.*, vol. 7, no. 1, p. 106, 1998.
- [5] S. Greek, F. Ericson, S. Johansson, M. Furtch, and A. Rump, "Mechanical characterization of thick polysilicon films: Young's modulus and fracture strength evaluated with microstructures," *J. Micromech. Microeng.*, vol. 9, no. 3, p. 245, 1999.
- [6] S. P. Baker and W. D. Nix, "Mechanical properties of compositionally modulated au-ni thin-films: nanoindentation and microcantilever deflection experiments," *J. Mater. Res.*, vol. 9, no. 12, p. 3131, 1994.
- [7] K. E. Petersen, "Young's modulus measurement of thin films using micromechanics," *J. Appl. Phys.*, vol. 50, p. 6761, 1979.
- [8] L. Kiesewetter, J.-M. Zhang, D. Houdeau, and A. Steckenborn, "Determination of Young's moduli of micromechanical thin films using the resonance method," *Sensors Actuators A*, vol. 35, p. 153, 1992.
- [9] Q. Zou, Z. Li, and L. Liu, "New methods for measuring mechanical properties of thin films in micromachining: beam pull-in voltage method (V_{pi}) and long beam deflection (LBD) method," *Sensors Actuators A*, vol. 48, p. 137, 1995.
- [10] P. M. Osterberg and S. D. Senturia, "M-TEST: A test chip for MEMS material property measurement using electrostatically actuated test structures," *J. Microelectromech. Syst.*, vol. 6, p. 107, June 1997.
- [11] E. K. Chan, K. Garikipati, and R. W. Dutton, "Comprehensive static characterization of vertical electrostatically actuated polysilicon beams," *IEEE Design Test Comput.*, vol. 16, p. 58, 1999.
- [12] J.-Å. Schweitz, "Mechanical characterization of thin films by micromechanical techniques," *MRS Bull.*, vol. 17, no. 7, p. 34, 1992.
- [13] W. N. Sharpe, S. B. Brown, G. C. Johnson, and W. G. Knauss, "Round robin tests of modulus and strength of polysilicon," in *Mater. Res. Soc. Proc.*, vol. 518, San Francisco, CA, 1998, pp. 57–65.
- [14] W. A. Brantley, "Calculated elastic constants for stress problems associated with semiconductor devices," *J. Appl. Phys.*, vol. 44, no. 1, p. 534, 1973.

- [15] D. Maier-Schneider, A. Koepf, S. B. Holm, and E. Obermeier, "Elastic properties and microstructure of LPCVD polysilicon films," *J. Micromech. Microeng.*, vol. 6, p. 436, 1996.
- [16] R. K. Gupta, "MIT, Electrostatic pull-in test structure design for in-situ mechanical property measurement of MEMS," Ph. D. dissertation, Massachusetts Inst. Technol (MIT), Cambridge, MA, 1997.
- [17] T. Yi and C.-J. Kim, "Measurement of mechanical properties for MEMS materials," *Meas. Sci. Technol.*, vol. 10, no. 706, 1999.
- [18] R. J. Hohlfelder, T. A. Friedmann, and J. P. Sullivan, "Measurement of the elastic modulus of tetrahedral amorphous carbon and polysilicon by cantilever beam deflection, 2001, to be published.
- [19] T. A. Lober, J. Huang, M. A. Schmidt, and S. D. Senturia, "Characterization of the mechanisms producing bending moments in polysilicon micro-cantilever beams by interferometric deflection measurements," in *Proc. Hilton Head '88*, Hilton Head, NC, 1988, pp. 92–95.
- [20] W. Fang and J. A. Wickert, "Comments on measuring thin-film stresses using bi-layer micromachined beams," *J. Micromech. Microeng.*, vol. 5, p. 276, 1995.
- [21] —, "Determining mean and gradient residual stresses in thin films using micromachined cantilevers," *J. Micromech. Microeng.*, vol. 6, p. 301, 1996.
- [22] B. D. Jensen, M. P. de Boer, and S. L. Miller, "IMaP: Interferometry for materials property evaluation in MEMS," in *Proc. MSM '99*, San Juan, Puerto Rico, 1999, pp. 206–209.
- [23] B. D. Jensen, M. P. de Boer, and F. Bitsie, "Interferometric measurement for improved understanding of boundary effects in micromachined beams," in *Proc. SPIE*, vol. 3875, Santa Clara, CA, 1999, pp. 61–72.
- [24] J. J. Sniegowski and M. P. de Boer, "IC-compatible polysilicon surface micromachining," *Annu. Rev. Mater. Sci.*, vol. 30, p. 297, 2000.
- [25] G. R. Fowles, *Introduction to Modern Optics*, 2nd ed. New York: Holt, Rinehard and Winston, 1975.
- [26] J. L. Devore, *Probability and Statistics for Engineering and the Sciences*, 2nd ed. Belmont, CA: Wadsworth, 1987.
- [27] B. L. Adams, S. I. Wright, and K. Kunze, "Orientation imaging: the emergence of a new microscopy," *Metall. Trans. A*, vol. 24A, no. 4, p. 819, 1993.
- [28] E. Brandes, *Smithells Metals Reference Book*, 6th ed. London, U.K.: Butterworths, 1983.
- [29] M. P. de Boer, N. F. Smith, N. D. Masters, M. B. Sinclair, and E. J. Prynputniewicz, "Integrated platform for testing MEMS mechanical properties at the wafer scale by the IMaP methodology," in *Mechanical Properties of Structural Thin Films*, STP no. 1413, S. B. Brown and C. L. Muhlstein, Eds. West Conshohocken, PA: ASTM, 2001, to be published.
- [30] M. P. de Boer and T. A. Michalske, "Accurate method for determining adhesion of cantilever beams," *J. Appl. Phys.*, vol. 86, no. 2, p. 817, 1999.
- [31] M. P. de Boer, P. J. Clews, B. K. Smith, and T. A. Michalske, "Adhesion of polysilicon microbeams in controlled humidity ambients," in *Mater. Res. Soc. Proc.*, vol. 518, San Francisco, CA, pp. 131–136.
- [32] M. P. de Boer, J. A. Knapp, T. A. Michalske, U. Srinivasan, and R. Maboudian, "Adhesion hysteresis of silane coated microcantilevers," *Acta Mater.*, vol. 48, no. (18–19), p. 4531, 2000.
- [33] M. P. de Boer, J. M. Redmond, and T. A. Michalske, "A hinged-pad test structure for sliding friction measurement in micromachining," in *Proc. SPIE*, vol. 3512, Santa Clara, CA, 1998, pp. 241–250.
- [34] B. T. Crozier, M. P. de Boer, J. M. Redmond, D. F. Bahr, and T. A. Michalske, "Friction measurement in MEMS using a new test structure," in *Mater. Res. Soc. Proc.*, vol. 605, Boston, MA, 2000, pp. 129–134.
- [35] M. P. de Boer, B. D. Jensen, and F. Bitsie, "A small area in-situ MEMS test structure to measure fracture strength by electrostatic probing," in *Proc. SPIE*, vol. 3875, Santa Clara, CA, 1999, pp. 97–103.



Brian D. Jensen received the M.S. degree in mechanical engineering from Brigham Young University (BYU), Provo, UT, in 1998 and is currently working towards the Ph.D. degree in mechanical engineering at the University of Michigan, Ann Arbor.

From May 1998 to August 1999, he worked in the MEMS and Novel Silicon Science & Technology Department at Sandia National Laboratories, Albuquerque, NM. His research interests include design of novel microactuators, multidomain modeling of microsystems, and optimization-based design of MEMS. He is currently a National Science Foundation Graduate Research Fellow.



Maarten P. de Boer received the Ph.D. degree in materials science from the University of Minnesota, Minneapolis, in 1996, performing research in the area of thin-film adhesion.

Prior to receiving the Ph.D. degree, he worked at Hewlett-Packard in IC fabrication of advanced CMOS processes, with responsibilities in transistor design, characterization, and process integration. He is currently a Senior Member of the Technical Staff in the Surface Micromachining Department at Sandia National Laboratories, Albuquerque, NM.

He served as coorganizer for the Materials Science of MEMS Symposium at the 1999 and 2000 MRS fall meetings. His current interests are in the area of developing test structures, metrologies and mechanics to study mechanical and tribological properties in MEMS.



Nathan D. Masters received the B.S. degree in mechanical engineering from Brigham Young University (BYU), Provo, UT, in 1998 and is currently pursuing the M.S. degree in mechanical engineering at BYU, with concentration in MEMS and bistable mechanisms.

He worked at Sandia National Laboratories, Albuquerque, NM, for a year-long internship, during which he conducted research in MEMS.

Mr. Masters is a member of the Tau Beta Pi National Engineering Honors Society.



Fernando Bitsie received the Bachelor of Science degree in mechanical engineering from New Mexico State University, Las Cruces, in 1989 and the Master of Science and Ph.D. degrees in mechanical engineering from Purdue University, West Lafayette, IN, in 1990 and 1996, respectively.

He is currently a Senior Member of the Technical Staff at Sandia National Laboratories, Albuquerque, NM. He has been involved in various microsystem inertial sensor projects in areas such as design and analysis. Previously, he has worked on several high-reliability electromechanical components for nuclear weapons.

Besides mechanical design, he has experience in finite element analysis of dynamic and electrostatic sensors.



David A. LaVan received the B.S. degree from the Materials Science Department and the M.S. degree from the Mechanical Engineering Department from the University of Florida, Gainesville. He received the Ph.D. degree in mechanical engineering from the Johns Hopkins University, Baltimore, MD, in mechanics of materials and microscale testing.

He completed a Postdoctoral Fellowship at Sandia National Laboratories, Albuquerque, NM, in the Materials Science and Processing Center. He worked on materials characterization and novel microscale testing techniques for MEMS.

He is currently a Research Fellow in the Surgical Research Department at Children's Hospital/Harvard Medical School and jointly a Research Affiliate in the Health, Sciences, and Technology Division at the Massachusetts Institute of Technology (MIT), Cambridge. His web address is: <http://www.mdl.sandia.gov/Micromachine>